Starvation and recovery in the deep-sea methanotroph *Methyloprofundus sedimenti*

Patricia L. Tavormina,[1]* Matthias Y. Kellermann,[2]
Chakkiath Paul Antony,[3] Elitza I. Tocheva,[4,5]
Nathan F. Dalleska,[6] Ashley J. Jensen,[5]
David L. Valentine,[2] Kai-Uwe Hinrichs,[7]
Grant J. Jensen,[8] Nicole Dubilier[3] and
Victoria J. Orphan[1]

[1]*Division of Geological and Planetary Sciences,
California Institute of Technology, 1200 E. California
Blvd, Pasadena, CA 91125, USA.*
[2]*Department of Earth Science and Marine Science
Institute, University of California, Santa Barbara,
CA 93106, USA.*
[3]*Max Planck Institute for Marine Microbiology,
Celsiusstraße 1, Bremen, 28359, Germany.*
[4]*Department of Stomatology and Department of
Biochemistry and Molecular Medicine, Université de
Montréal, P. O. Box 6128 Station Centre-Ville,
Montreal, QC H3C 3J7, Canada.*
[5]*Division of Biology and Biological Engineering and,
California Institute of Technology, 1200 E. California
Blvd, Pasadena, CA 91125, USA.*
[6]*Environmental Analysis Center, California Institute of
Technology, 1200 E. California Blvd, Pasadena, CA
91125, USA.*
[7]*MARUM Center for Marine Environmental Sciences,
University of Bremen, Leobener Str, Bremen, 28359,
Germany.*
[8]*Division of Biology and Biological Engineering and
Howard Hughes Medical Institute, California Institute
of Technology, 1200 E. California Blvd, Pasadena, CA
91125, USA.*

Summary

In the deep ocean, the conversion of methane into derived carbon and energy drives the establishment of diverse faunal communities. Yet specific biological mechanisms underlying the introduction of methane-derived carbon into the food web remain poorly described, due to a lack of cultured representative deep-sea methanotrophic prokaryotes. Here, the response of the deep-sea aerobic methanotroph *Methyloprofundus sedimenti* to methane starvation and recovery was characterized. By combining lipid analysis, RNA analysis, and electron cryotomography, it was shown that *M. sedimenti* undergoes discrete cellular shifts in response to methane starvation, including changes in headgroup-specific fatty acid saturation levels, and reductions in cytoplasmic storage granules. Methane starvation is associated with a significant increase in the abundance of gene transcripts pertinent to methane oxidation. Methane reintroduction to starved cells stimulates a rapid, transient extracellular accumulation of methanol, revealing a way in which methane-derived carbon may be routed to community members. This study provides new understanding of methanotrophic responses to methane starvation and recovery, and lays the initial groundwork to develop *Methyloprofundus* as a model chemosynthesizing bacterium from the deep sea.

Introduction

Methane in the deep ocean, metabolized by chemosynthetic methane-oxidizing bacteria in family *Methylococcaceae*, provides a primary source of energy and carbon to seafloor communities (Reeburgh, 2007). Chemosynthesis from methane contributes directly to the trophic base of seafloor communities through multiple routes, including through methanol production supporting non-methanotrophic bacteria, biomass production supporting protozoal grazers, and through symbiotic relationships with invertebrate animals (reviewed in Fisher, 1996; Levin, 2005). Deep-sea *Methylococcaceae* have not been developed as model organisms despite the multiple ecological services they provide, and this deficiency limits our ability to investigate how methane sustains diverse deep-sea faunal communities. Such a model system would allow independent estimation of the contribution of methane to deep-sea communities, complementing estimates from culture-free methods

(reviewed in Levin, 2005). This in turn would expand our understanding of carbon flow in methane seep communities much as development of *Prochlorococcus* provides ongoing invaluable insight into the flow of carbon in sunlit surface waters (reviewed in Biller *et al.*, 2015).

Methane levels at cold methane seeps vary intermittently from nanomolar to millimolar concentrations (Reeburgh, 2007, see also Ruff *et al.*, 2013; Grupe *et al.*, 2015). Because of this variability, deep-sea methane-oxidizing *Methylococcaceae* are expected to employ mechanisms to adapt to methane limitation (starvation) and variability (flux), however, these expected mechanisms have not been explored. The starvation response among heterotrophic proteobacteria (e.g., *Escherichia* and *Vibrio* spp.) includes changes in membrane composition, reduction in cytoplasmic volume, depletion of biosynthetic intermediates, and maintenance of membrane-bound transporters (reviewed in Siegele and Kolter, 1992; Kolter *et al.*, 1993; Ksiazek, 2010). These responses alter the fluidity and permeability properties of membranes, physically stabilize cells, and promote cellular competition for nutrients (Oliver and Stringer, 1984; Hood et al., 1986; Kjelleberg *et al.*, 1993; Foster and Spector, 1995; Houser et al., 2015; Ksiazek, 2010). Chemosynthesizing bacteria in *Methylococcaceae* rely heavily on membrane-associated metabolism, most notably for the oxidation of methane to methanol as a first step in energy and carbon acquisition. Indeed, the biological centrality of methane metabolism to *Methylococcaceae* is evidenced, in part, by the extensive intracytoplasmic membrane that houses the enzyme that catalyzes methane oxidation, the particulate methane monooxygenase (pMMO, *pmo*).

We previously reported a new deep-sea methane-oxidizing methanotroph (*Methyloprofundus sedimenti* strain WF1; Tavormina *et al.*, 2015). Members of genus *Methyloprofundus* inhabit a range of marine settings including sediments, the water column, and within bacteriocytes of *Bathymodiolus* mussels (Tavormina *et al.*, 2015 and references therein). Because of this distribution across multiple ecological niches, *M. sedimenti* is an excellent candidate for development as a deep-sea chemosynthetic model organism. Toward this end, the present work describes the response of *M. sedimenti* to fluctuating methane levels, and includes quantitation of lipid, transcriptional, and morphological shifts during active growth, methane starvation, and methane replenishment. Our findings reveal unique lipid modulation during the transition from active growth to methane starvation, elevated levels of *pmo* transcripts during methane starvation, and transient accumulation of extracellular methanol upon methane replenishment. In whole, this work provides a foundation to develop *M. sedimenti* into a model chemosynthetic bacterium from the deep sea.
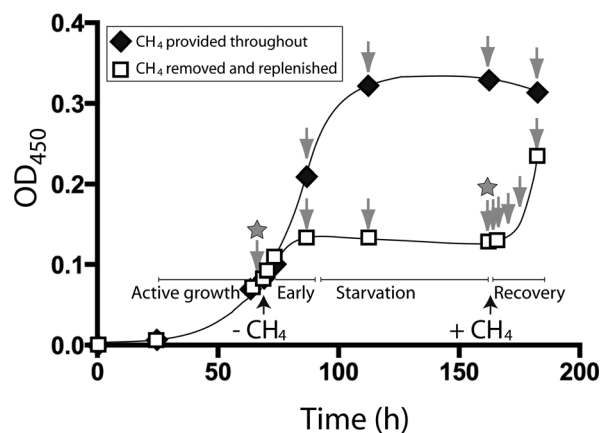
Fig. 1. Growth curve and sampling scheme. Growth kinetics follow four replicates; T_0 = inoculation of frozen stock culture into fresh media. Growth for *Methyloprofundus sedimenti* during incubation with methane (upper curve, filled diamonds) and during a round of methane starvation and recovery (lower curve, open squares) is shown. Time points for removal of methane (70 h) and replenishment of methane (166 h) are indicated with black arrowheads. Time points sampled for transcriptional analysis are indicated with grey arrowheads. Time points sampled for lipid analysis and electron cryotomography are indicated by stars.

Results and discussion

To characterize the response of *M. sedimenti* to intermittent methane supply, we evaluated select cellular features during growth in the presence of methane, during a time course of methane starvation, and during a time course following the reintroduction of methane to starved cells (Fig. 1). Our analyses included determination of membrane lipid headgroup speciation and fatty acid saturation, quantitation of transcripts involved in select metabolic pathways including methane oxidation, and quantitation of methanol accumulation in culture media. Additionally, electron cryotomography provided morphological context in support of key findings.

General growth characteristics

Methane-dependent growth kinetics of *M. sedimenti* were monitored to characterize periods of active growth and entry to stationary phase, entry to starvation in the absence of methane, and resumption of growth upon the reintroduction of methane. When grown in the presence of methane, cells doubled every 13 h. Cultures transitioned from logarithmic growth to early saturation at an optical density (OD_{450}) of $\sim$ 0.28, and reached a final OD_{450} of $\sim$ 0.35 (Fig. 1).

Methane starvation was induced during active growth ($OD_{450} = 0.085 \pm 0.002$) by removing stoppers from culture vessels and loosely covering vessels with sterile caps. Inducing starvation in this manner caused growth to slow within 9 h and to cease within 18 h ('early

starvation,' OD$_{450}$ = 0.135 ± 0.002). Between 18 and 96 h ('starvation'), the optical density diminished slightly (OD$_{450}$ = 0.130 ± 0.002). Sealing the bottle and resupplying methane to the culture vessel at 96 h prompted resumption in growth within 4 h ('recovery'), and these recovered cultures grew to saturation following normal growth kinetics. Cells were sampled throughout this time course for multiple analyses, as indicated in Fig. 1.

Lipid-based adaptations during active growth and starvation

In chemoheterotrophic bacteria, lipid composition is dependent on growth state and nutritional status. Among these organisms (e.g., *E. coli* and *Vibrio* spp.) nutrient depletion is accompanied by a decrease in phosphatidylethanolamine (PE), and an increase in both cardiolipin (CL) and in fatty acid (FA) saturation (Oliver and Stringer, 1984; Hood et al., 1986; Linder and Oliver, 1989; DiRusso and Nystrom, 1998). Functionally, these changes decrease membrane permeability and stabilize transport processes (Nystrom, 2004). Among methanotrophic bacteria, the initial step of carbon and energy metabolism is membrane-bound; thus, preservation of membrane function (i.e., fluidity and permeability properties sufficient to enable metabolism) during starvation may be necessary, to facilitate starvation recovery. We analyzed lipids from actively growing and starved cells to investigate this possibility. We assessed molecular features of both the polar lipid fraction (lipid headgroups) and the fatty acid tails (FAs; molecular structures identified in this study are provided in Supporting Information Fig. S1).

Headgroup analysis

Polar lipid headgroup components of *M. sedimenti* were remarkably constant between active growth and starvation, with one notable exception. The glycerolipids phosphatidylethanolamine (PE, ~ 75%) and phosphatidylglycerol (PG, ~ 18%) were the dominant constituents under both conditions (Fig. 2A). Cardiolipin (CL, < 1%), on the other hand, increased ~ 8-fold (from 0.07% to 0.54%) during starvation. Cardiolipin is associated with multiple functions in prokaryotes, including response to stress and respiration (Romantsov et al., 2009; see also Arias-Cartin et al., 2012 for a focused review of the role of cardiolipin in bacterial respiratory complexes). Other minor lipids, including methylene-ubiquinone (M-UQ ~ 3%, cf., Collins and Green, 1985) and a component resembling a cyanobacterial heterocyst-like glycolipid (HC-G < 1%; Supporting Information Fig. S1), remained constant under both conditions (Fig. 2A).
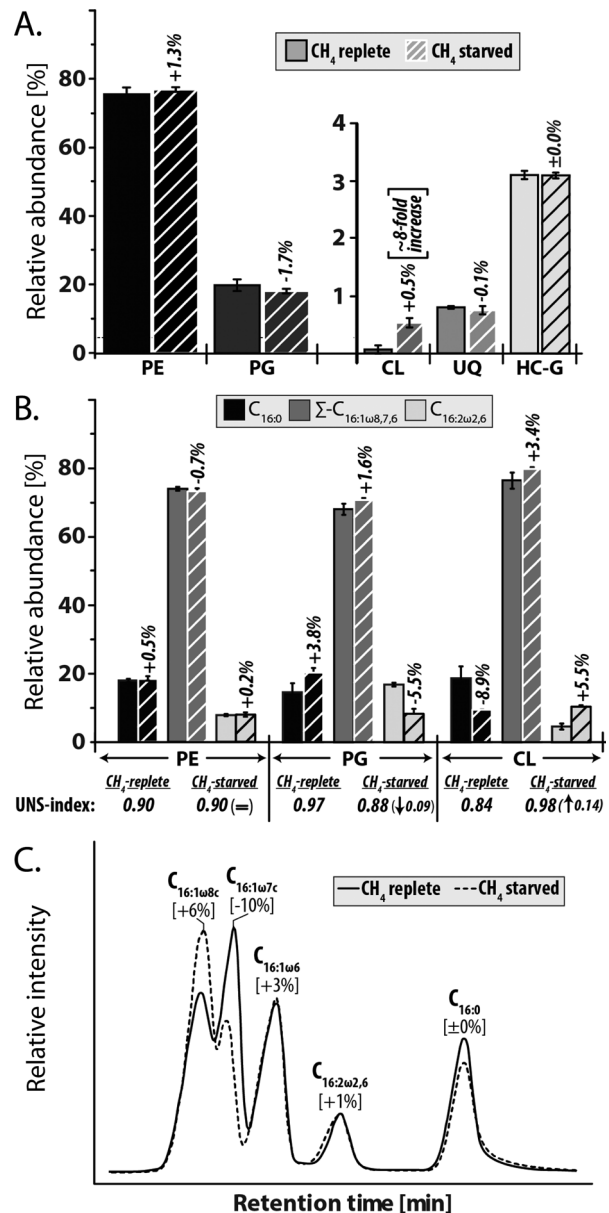
Fig. 2. Lipid analysis of *M. sedimenti*. Panel A: Polar lipid composition. Panel B: Headgroup specific fatty acid composition (phosphatidylethanolamine, PE; phosphatidylglycerol, PG; cardiolipin, CL; Heterocyst-like glycolipid, HC-G; and Ubiquinone, UQ). Panel C: A representative chromatogram showing the relative abundance of specific fatty acids released from precursor glycerolipids after acid hydrolysis. All analyses were performed in triplicate.

Electron cryotomography imaging of *M. sedimenti* showed that extensive intracellular membrane (ICM) stacks account for > 85% of cellular membrane during both active growth and starvation (Supporting Information Fig. S2). Methane is highly transient in the deep sea as a result of tides, sub-seafloor processes, seismic activity or changes in ocean currents (e.g., Krabbenhoeft et al., 2010; Von Deimling et al., 2010). Data presented

here demonstrates that membrane composition at the gross morphological as well as the molecular level is maintained during a 96 h starvation course in *Methylopro-fundus*, drawing a contrast with other bacterial systems, and consistent with the centrality of membrane-based metabolism for carbon and energy acquisition in bacterial methanotrophs.

Detailed FA analysis of the glycerolipids PE, PG and CL

Polar headgroup speciation did not change markedly during starvation; however, shifts were measured in the saturation levels of specific fatty acid chains. During star-vation, PE ($\sim$ 75% of bulk lipids) retained constant FA composition (unsaturation index, 'UNS-index', of $\sim$ 0.90). PG and CL showed opposing responses in their FAs sat-uration. During starvation, unsaturation decreased in PG (UNS-index from 0.97 to 0.88), and increased in CL (UNS-index from 0.84 to 0.98; Fig. 2B). Changes in FA unsaturation was particularly noticeable in the polyunsa-turated FA (PUFA) $C_{16:2\omega2,6}$, decreasing from 14% to 8% in PG and increasing from 4% to 10% in CL (Fig. 2B). Of note, among cultivated aerobic methanotrophs, *M. sedimenti* is the only representative known to synthesize significant $C_{16:2}$ PUFAs ($\sim$ 7% of total FAs; Fig. 2B and Supporting Information Fig. S3); although members of *Methylocystaceae* have been shown to synthesize $C_{18:2}$ PUFAs (Bodelier *et al.*, 2009).

Bulk FA analysis also demonstrated that double bonds within mono-unsaturated fatty acids (MUFAs, i.e., $C_{16:1\omega8}$, $C_{16:1\omega7}$, $C_{16:1\omega6}$, 73% of total FAs) were located near the geometric centre of the hydrocarbon chain (Fig. 2C). Such placement perturbs van der Waals chain–chain interaction, resulting in the lowest possible melting points and highest possible fluidity within the membrane bilayer (Koynova and Caffrey, 1998). Shifts in abundances of $C_{16:1\omega8}$ and $C_{16:1\omega7}$ also occurred during starvation (Fig. 2C).

If membrane function *per se* is fundamentally impor-tant to methanotroph physiology, then restoring fatty acid desaturations, with a predicted increase in mem-brane fluidity and permeability, will be an early step in the recovery from methane starvation. In support of this hypothesis, a transient 45-fold increase in the expres-sion of FA desaturase was measured within 10 min of methane's reintroduction (Fig. 3). A similar spike of lesser magnitude was observed in the expression of FA cis-trans isomerase (Supporting Information Table S1). These data show that membranes in *M. sedimenti* adapt dynamically to transient methane supply, consistent with the view that membrane function is critical to methane metabolism.
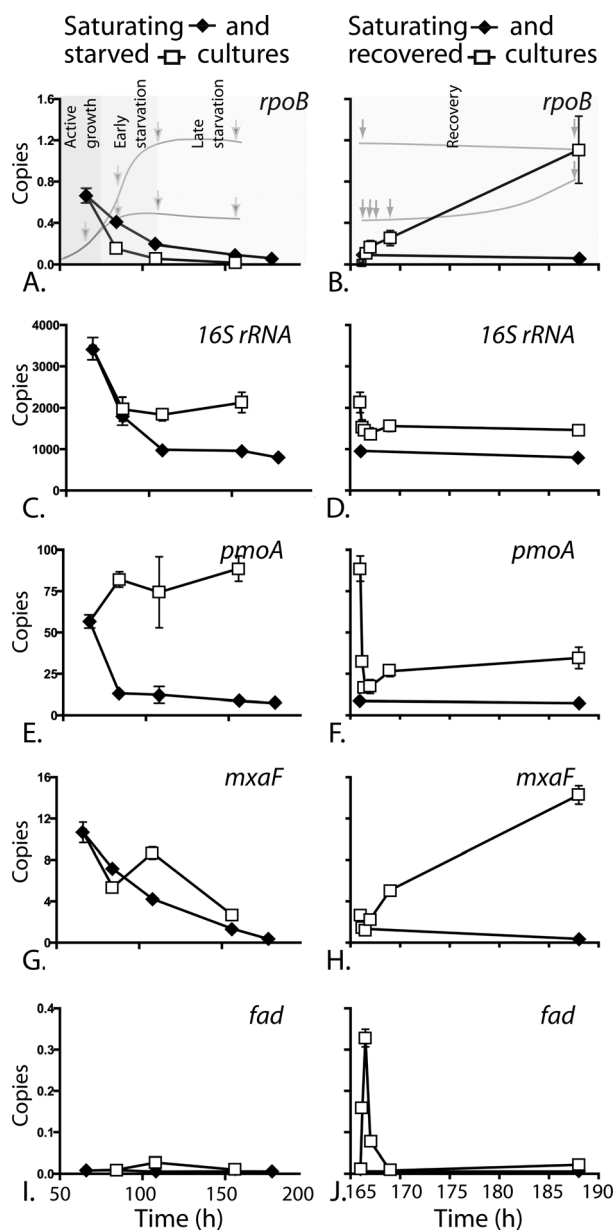
Fig. 3. Transcript abundances (copies per cell) during methane starvation (A, C, E, G, I) and recovery (B, D, F, H, J). Panels A, B: For the housekeeping gene *rpoB*, transcripts declined as cultures saturated (+ methane), but declined more steeply when starved. Transcripts rose steadily during recovery. Panels C, D: 16S rRNA gene transcripts. Ribosomal RNA transcripts declined during culture saturation (+ methane); starving cultures retained higher numbers of ribosomal RNA transcripts. Panels E, F: Transcripts for *pmoA* (particulate methane monooxygenase) declined during culture saturation (+ methane). Of note, *pmoA* transcript abundance was significantly elevated during starvation. Recovery from starvation was accompanied by a rapid decrease in *pmoA* transcript abundance. Panels G, H: Transcripts for *mxaF* (methanol dehydrogenase) declined during saturation (+ methane). During starvation, transcript levels generally declined, with a transient spike in abundance at 48 h. Transcripts rose steadily during recovery. Panels I, J: Transcripts for *fad*, a delta-9 fatty acid desaturase, spiked dramatically during the first 10 min of recovery from starvation. Information for additional gene targets is provided in Supporting Information Table S1.

Expression of select genes during starvation and recovery

Among aerobic methanotrophs, methane metabolism begins directly on membranes, via the action of particulate methane monooxygenase (pMMO, *pmo*). The conservation of membrane lipids and ICM during starvation, and the rapid upshift in expression of fatty acid desaturase upon methane replenishment, led us to hypothesize that starved *M. sedimenti* cells are well-poised to respond to methane. If so, expression of *pmo* genes may be uniquely regulated toward this same end, to facilitate rapid methane metabolism upon methane flux. We measured transcript abundances for the *pmoA* and *pmoC* genes to test this hypothesis. While transcript abundance should not be confused with enzymatic function, this approach provides insight into the genetic programming underlying the response of cells to their environments.

We measured expression of *pmoA* and *pmoC* (whose protein products comprise two subunits of pMMO) during active growth, starvation, and recovery. We concurrently measured expression of genes encoding methanol dehydrogenases (MDH, *mxaF* and *xoxF*), which catalyze the conversion of methanol to formaldehyde. It is worth noting that *xox*-encoded MDHs rely on lanthanides for function (Keltjens *et al.*, 2014; Pol *et al.*, 2014), which were not included in this study. Lanthanides are present in many ocean sediments (Kato *et al.*, 2011), suggesting that these metals may be relevant to the biology of deep-sea methanotrophs. We also measured expression of genes involved in central metabolic pathways, fatty acid metabolism, 'housekeeping' functions and the 16S rRNA gene.

Actively growing cells demonstrated exceptionally high transcript levels for the 16S rRNA gene and *pmo* genes, high transcript levels for genes related to methanol utilization, and lower transcript levels for other metabolic and housekeeping genes (e.g., fatty acid desaturase, PEP carboxylase, glycogen debranching enzyme, polysaccharide deacetylase and *rpoB*; Fig. 3, Supporting Information Table S1). During starvation, transcript levels for virtually every gene assessed reduced significantly. This reduction was apparent within 18 h of starvation and was near-complete for most targets by 48 h starvation.

However, transcript abundances for *pmoA* and *pmoC* significantly increased during starvation (Fig. 3E, Supporting Information Table S1), and these abundances remained high throughout the starvation time course. While this increase could reflect scavenging of trace methane, it is worth noting that transcripts encoding methanol dehydrogenases (*mxa* and *xox*), like most other gene transcripts assessed here, generally declined during the 96 h

starvation course (Fig. 3G, Supporting Information Table S1). An alternative interpretation is that increased *pmo* transcript abundance is part of cellular program to facilitate re-entry to growth upon methane replenishment. In some ammonia oxidizing bacteria including members of *Nitrosospira*, transcripts encoding the evolutionarily-related ammonia monooxygenase (AMO, *amo*) are slowly degraded during a 12 day course of ammonia starvation, compared with the bulk of cellular mRNAs (Bollmann *et al.*, 2005). These evolutionarily-related monooxygenases may, as a group, encode stable mRNAs.

Our data also demonstrate that transcripts for methane monooxygenase and methanol dehydrogenase were independently regulated during starvation. Specifically, *pmo* transcript levels increased while *mxa* and *xox* transcript levels decreased. To our knowledge, a strategy of increasing methane monooxygenase transcripts in the absence of methane has not previously been demonstrated.

An important implication of these data bears upon the correct interpretation of environmental transcriptomic datasets. The abundance of environmental *pmo* transcripts has been used as a proxy for methane oxidation (e.g., Rivers *et al.*, 2013; Li *et al.*, 2014), but the underlying assumption – that *pmo* transcript abundance declines in the absence of methane – had not been formally tested. Data here demonstrate that *pmo* transcripts are most abundant when the cells are in a state of starvation. Environmental *pmo* transcript abundances are best interpreted within the context of methane concentrations and oxidation rates, as well as the abundances of additional gene transcripts, such as those for methanol dehydrogenase.

We also assessed expression of these gene targets during recovery from starvation. Transcripts for the *rpoB* housekeeping gene (Case *et al.*, 2007) steadily increased over the recovery time course (Fig. 3B). In contrast, transcript abundances for fatty acid desaturase and fatty acid isomerase spiked and fell within 10 min of methane availability (Fig. 3J, Supporting Information Table S1), providing evidence that remodeling of membrane lipids is an early step in recovery from methane starvation. By 20 h recovery, most gene transcript levels were within two-fold of their pre-starvation levels (Figs. 3 and 4, Supporting Information Table S1).

Notably, within 30 min of methane reintroduction, transcripts for *pmo* genes decreased by a factor of 6 (Fig. 3F), demonstrating that transcripts present during starvation were degraded during recovery at a rate that exceeded *de novo* synthesis. The biological implications of a decrease in *pmo* transcript abundance during early recovery from starvation are not clear. However, like the increase in transcript abundance observed during starvation, this finding directly relates to the correct interpretation of environmental transcriptomic datasets, and how accurately these datasets reflect environmental function.
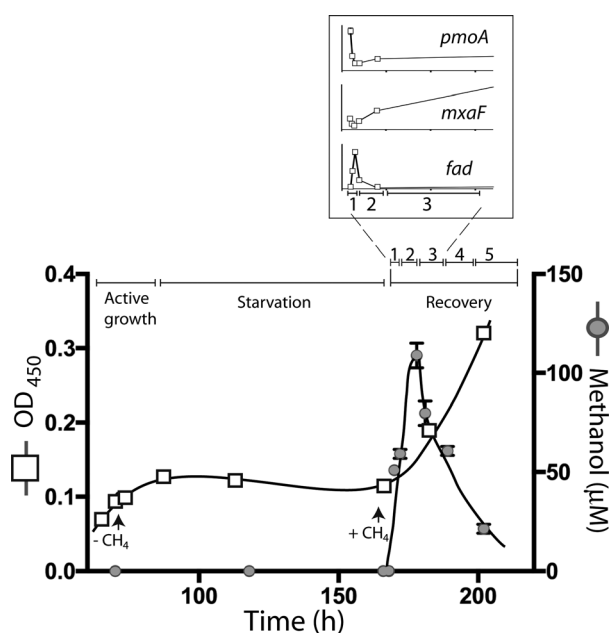
Fig. 4. Recovery from starvation: Culture density, methanol production, and select gene transcript abundances (inset; see also Fig. 4). Within 60 min of methane availability (stage 1), *pmoA* transcript abundances decreased by 65%, while transcripts for fatty acid desaturase increased approximately 45-fold. Between 1 and 4 h of methane availability (stage 2), culture density increased and methanol was detected, indicating active methane metabolism. Between 4 and 12 h of methane availability (stage 3), methanol production exceeded utilization. Between 12 and 36 h of methane availability (stage 4), methanol levels decreased, suggesting coordinated methane and methanol metabolism. By 36 h (stage 5), cells had reentered logarithmic growth and most gene targets were within two fold of their pre-starvation levels.

Elevated methanol concentrations during recovery

The maintenance of membrane features and *pmo* transcripts during starvation, with concurrent reduction in methanol dehydrogenase transcripts, led us to predict that during recovery, methane oxidation will outpace methanol utilization. Bacterial methanotrophs contribute to the food web through conversion of methane to methanol, which can be further metabolized to formaldehyde and complex organic carbon. Thus, methanotrophs provide an ecological service by generating biologically available carbon for non-methanotrophic methylotrophs, and also for grazers. Indeed, non-methanotrophic methylotrophs (e.g., *Methylotrichales* and *Methylophilales*) are identified in methane stable isotope probing (SIP) of deep-sea sediments (Redmond *et al.*, 2010; see also Jensen *et al.*, 2008), demonstrating that methane-derived carbon readily flows to non-methanotrophic community members. The presence of *Methylophaga* in *Bathymodiolus heckerae* gill tissue provides another line of evidence for an ecological association between methanotrophs and methylotrophs in the deep sea (Duperron *et al.*, 2007). Methanol not only feeds non-methanotrophic methylotrophs, but also

positively regulates methanotroph function: methane uptake by methanotrophic cells is stimulated by methanol in some systems (Benstead *et al.*, 1998).

We measured methanol in culture media to determine if methane oxidation outpaces methanol utilization during recovery. Under conditions used here, methanol concentrations were below detection during active growth and starvation. However, during the first 12 h of recovery from starvation, methanol accumulated in the growth media to concentrations over 100 μM (Fig. 4). This result demonstrates that methane was oxidized within hours of its availability, and further demonstrates that methane oxidation outpaced methanol utilization during early recovery, consistent with mRNA expression patterns. From an ecological perspective, this suggests that a methane flux event in deep-sea ecosystems may lead to a methanol pulse to associated community members, offering a newly-conceived route for methane-derived carbon transfer *in situ*. However, because the activity of some *xox*-encoded methanol dehydrogenase depends on lanthanides (Keltjens *et al.*, 2014; Pol *et al.*, 2014), the pulse of methanol observed in this study could be less relevant in deep-sea environments.

Cell morphological changes during active growth and starvation

The lipid, transcriptional, and physiological responses of *M. sedimenti* during growth and starvation were placed within cell morphological context using electron cryotomography (ECT, Tocheva *et al.*, 2010). Besides the measurements related to intracytoplasmic membranes noted above, storage granule and periplasmic features shifted during growth and starvation. The imaging in this study represents the first electron cryotomographic imaging of a proteobacterial methanotroph, providing context in which to consider the stress response of a deep-sea methane oxidizing bacterium.

A clear morphological change during starvation was a visible increase in the periplasmic volume, and the volume between every second ('alternating') stacked membrane layer (Fig. 5). The absolute diameter of growing and starved cells was essentially unchanged, thus this increase in periplasmic space was most likely due to a decrease in cytoplasmic volume. A decrease in cytoplasmic volume is a well-established response to starvation among model chemoheterotrophs, and is thought necessary to maintain concentrations of cytoplasmic compounds (Siegele and Kolter, 1992). The same principle may underlie the starvation-associated decrease in cytoplasmic volume observed here. ECT also revealed a studded surface layer (S-layer) around the periphery of cells, during both active growth and starvation (Fig. 5).
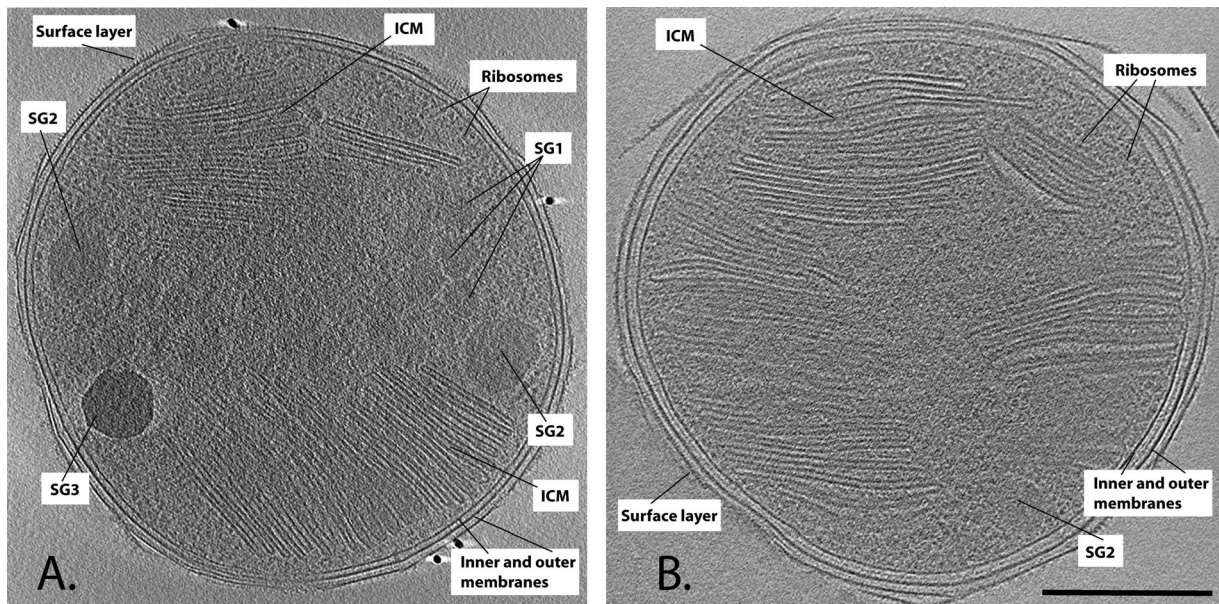
Fig. 5. Electron cryotomographic views of *Methyloprofundus sedimenti* during active growth and starvation. Panel A: Active growth. Intracytoplasmic membranes (ICM) occupy most of the cell interior. Storage granules are seen and include abundant, small, lobed granules (SG1), slightly larger and denser granules (SG2) and highly electron-dense granules (SG3). A typical diderm cell envelope and a surface layer are observed. Panel B: Starvation. SG1 is no longer detected. SG2 is occasionally detected. SG3, although outside the imaged plane in this view, remains present in all cells (see Supporting Information Movie S2.). The periplasmic space and space between alternating membrane stacks increases in volume, indicating a reduction in cytoplasmic volume. Scale bar: 500 nm.

In starved cells the S-layer was fragmented at multiple points along the cell surface. S-layers are common among prokaryotes, participate in multiple functions, and have been reported from several methanotrophic genera (Lindner *et al.*, 2007; Khmelenina *et al.*, 2010, 2013; Wu *et al.*, 2012).

Within actively growing cells, three storage granule types were observed (Fig. 5A; Supporting Information Figs. S2, and S4; Supporting Information Movies S1 and S2). The identities of these granules are not yet known, but may be estimated from appearance, response to starvation, and genomic potential. During active growth, lobular granules filled the cell ('SG1', Fig. 5A). These were of a size and density typical of glycogen (see Liberton *et al.*, 2011), a common prokaryotic storage compound often consumed during starvation (Iglesias and Preiss, 1992; Wang and Wise, 2011). After 96 h of methane starvation, these granules were absent (Fig. 5B). The genome of *M. sedimenti*, and the genomes of closely related uncultivated methane-oxidizing endosymbionts of *Bathymodiolus* mussels (Antony, unpublished data), encode a complete glycogen storage and utilization pathway, suggesting that a capability for glycogen utilization may occur across genus *Methyloprofundus*.

A second storage granule, present in ∼ 5–10 instances per cell during active growth, appeared as a larger and slightly more electron-dense elliptical structure ('SG2', Fig. 5). During starvation, these elliptical granules were occasionally detected at 1–2 instances per cell. The identity of these granules is unknown.

A third storage granule type appeared as large, electron-dense spheres, present in two or three instances per cell in non-dividing cells (Fig. 5A; Supporting Information Fig. S4, Supporting Information Movie S1). In dividing cells, these granules partition into daughter cells (Supporting Information Fig. S4, Supporting Information Movie S2). These granules have the characteristic appearance of polyphosphate (Tocheva *et al.*, 2013). Polyphosphate granules are highly electron dense, occur across all domains of life and perform functions including DNA partitioning, phosphorous storage, energy distribution, and virulence (reviewed in Rao *et al.*, 2009). The gene encoding polyphosphate kinase is present in the genome of *M. sedimenti*, and in numerous additional methanotroph genomes including the methanotrophic endosymbionts of *Bathymodiolus* (Antony, unpublished data). Polyphosphate has been demonstrated in members of *Methylocystis* (e.g., Lindner *et al.*, 2007), but a specific role has not been described. The number and location of electron-dense granules reported here, and the separation of these granules into daughter cells (Supporting Information Movie S2), provides evidence that these electron dense granules are associated with a partitioning function in *M. sedimenti*.

Conclusions

Chemosynthesis drives benthic faunal communities in the deep sea, yet little is known about the primary producers within these communities. Our work provides the first detailed description of the response of a deep-sea methane-oxidizing bacterium, *Methyloprofundus sedimenti*, to methane starvation and recovery. *M. sedimenti* was originally recovered from sediment near a whale fall, and is the closest cultured relative of the methane-oxidizing endosymbionts of *Bathymodiolus* mussels. Thus, insights from this work directly relates to a variety of deep-sea methane-fuelled communities, including sediments that have undergone organic loading from whale falls and methane seep environments that harbour *Bathymodiolus* mussel beds. Here we showed that within four days of methane starvation *M. sedimenti* membrane lipids became more highly saturated, but lipid headgroups did not appreciably change in abundances. Carbon storage granules were depleted during starvation, and transcripts relevant to methane oxidation were elevated. During early recovery from starvation extracellular methanol accumulated to concentrations exceeding 100 μM, revealing a biological route by which methane may become available to non-methanotrophic methylotrophs. This newly-described route for environmental carbon flow directly links an environmental methane flux event to an environmental methanol pulse. In sum, this work provides the first controlled experimentation into the response of a deep-sea bacterial methanotroph to transient methane supply, and begins to illuminate survival strategies and routes of biological carbon acquisition in deep-sea faunal communities.

Experimental procedures

Strain and growth conditions

Methyloprofundus sedimenti strain WF1 (ATCC BAA-2619[T], BCCM LMG 28393[T]) was grown on a modified version of nitrate mineral salts (NMS, ATCC 1306). Modifications included: Trace element solution from ATCC 1306 was replaced with trace element solution from medium DSM141 (Robb *et al.*, 1995), vitamin solution from medium DSM141 was added at a 1:1,000 dilution, and sodium chloride (NaCl) was added to a final concentration of 0.17 M (2% w/v). Cultures were grown in 2 L sealed bottles with liquid not to exceed 15% of vessel volume, and methane was added to 20% headspace volume. Methane was added in 60 mL aliquots with a needle and syringe, and 60 mL headspace aliquots were removed after alternate methane additions, such that the pressure in the bottle was maintained between 1 and 1.1 atmospheres. Cells were grown at 22°C with gentle rotation (Td = 13 h). Culture purity was verified in log, stationary, and recovery phases by fluorescent *in situ* hybridization (FISH, not shown) using probes and conditions described previously (Tavormina *et al.*, 2015).

Lipid analysis

Triplicate cultures (300 mL each) were inoculated from frozen cell stocks (=T_0) and grown to an OD_{450} of 0.085 (T = 70 h growth). About 100 mL samples were then transferred to a sterile flask, chilled with swirling on ice, and collected by centrifugation in paired 50 mL Falcon tubes (Thermofisher scientific, Waltham MA, USA). Pellets were drained of liquid and stored at −80°C until processing. The remaining culture volume (200 mL) was loosely capped without added methane (=initiation of methane starvation). After 96 h of starvation (T = 166 h), 100 mL samples were collected as above and stored at −80°C until processing.

Total lipid extracts (TLEs) were obtained from cell pellets using a modified Bligh and Dyer protocol (Sturt *et al.*, 2004), after adding an internal standard (phosphatidylcholine $C_{21:0/21:0}$) and 3 g of combusted sea sand. The obtained TLEs were stored at −20°C and analysis of intact polar lipids (IPLs) was performed by high-performance liquid chromatography electrospray ionization mass spectrometry (HPLC-ESI-MS). Separation of IPLs was achieved on a Dionex Ultimate 3000 UHPLC equipped with a Waters Acquity UPLC BEH Amide column (150 × 2.1 mm, 1.8 μm particle size). Chromatographic conditions, according to a previously published method (Wörmer *et al.*, 2013) were as follows: constant flow rate of 0.4 mL/min with eluent A (75% acetonitrile; 25% DCM; 0.01% formic acid; 0.01% ammonium hydroxide solution (NH_3 aq) and eluent B (50% MeOH; 50% Milli-Q water; 0.4% formic acid; 0.4% NH_3aq). Under a constant flow, the HPLC routine applied: 99% A and 1% B for 2.5 min, increasing to 5% B at 4 min, followed by a linear gradient to 25% B at 22.5 min and then to 40% B at 26.5 min. Thereafter a 1 min washing step with 40% B followed and afterward reset to the initial conditions for 8 min to achieve column re-equilibration. Compound detection was conducted on a Bruker maXis Ultra-High Resolution qToF-MS, equipped with an ESI interface. IPLs were measured in positive ionization mode, while scanning a mass-to-charge (m/z) range of 150–2,000, with automated data-dependent MS/MS fragmentation of base peak ions. Compound identification was achieved by monitoring exact masses of possible parent ions (present mainly as H^{+} and NH_4^+ adducts) in combination with characteristic fragmentation patterns (Sturt *et al.*, 2004; Yoshinaga *et al.*, 2011). Potential differences in the ionization of individual lipid classes during HPLC-MS routines were calibrated against commercially available or purified lipid standards and expressed relative to 1,2-dihenarachidoyl-sn-glycero-3-phosphocholine (C_{21}-PC, Avanti Polar Lipids Inc., USA).

For a detailed FAs analysis, a 20% aliquot of the total lipid extract was transmethylated with 2.5% methanolic HCl (3 h at 70°C) yielding fatty acid methylesters (FAMEs). FAMEs were identified on a gas chromatography–mass spectrometry (GC–MS) system (Thermo Electron Trace MS) and quantified using a flame ionization detector (FID), as described previously (Kellermann *et al.*, 2012).

RNA analysis

Replicate cultures (300 mL) were inoculated from frozen cell stocks (=T_0). After entering logarithmic growth phase

($OD_{450} = 0.085$, $T = 70$ h growth), 20 mL aliquots were sampled into an equal volume of RNAlater (Thermofisher scientific, Waltham MA, USA) and pelleted in an Eppendorf 5804R tabletop centrifuge at $2000g$ for 25 min. The remaining cell culture (280 mL) was split between two sterile 2 L bottles. One bottle was loosely capped without exogenous methane (=initiation of methane starvation), while the second bottle was stoppered and incubated with methane as above. At 18, 48 and 96 h starvation, a 20 mL sample was removed from each bottle into an equal volume of RNA later, pelleted, and stored as above. Recovery from starvation was initiated by stoppering the starved bottles and adding methane, as above. At 10 min, 30 min, 60 min, 3 h and 19 h recovery, a 20 mL sample was removed into an equal volume of RNA later, and pelleted and stored as above. Bottles that were not starved were sampled at the 19 h recovery time point. Cell pellets were stored at −80˚C until processing, within 2 weeks.

RNA isolation and cDNA generation

RNA was isolated from cell pellets using the RNAeasy midikit (Qiagen, Valencia, CA, USA) following manufacturer's guidelines with the following modification: After recovery of RNA, residual contaminating DNA was removed by incubation with RNAse-free DNAse set (Qiagen, Valencia, CA, USA) following manufacturer's guidelines. This preparation was subjected to a second RNAeasy midikit isolation to purify RNA from remaining nucleotides and DNAse. The final RNA preparation was quantified using a Nanodrop 3300 (Thermo Scientific, Wilmington, DE, USA) and 400 ng of RNA from each preparation were converted to cDNA using the High Capacity Reverse Transcription Kit (Applied Biosystems, Foster City CA, USA). Duplicate reactions containing no reverse transcriptase were included to estimate contaminating DNA in downstream manipulations; contaminating DNA was routinely negligible. Final cDNAs were diluted to 0.2 ng/μL and stored at −20˚C until processed in Real Time PCR, within 2 weeks.

Real time PCR

Real Time PCR was performed using a Biorad CFX96 Touch Real Time PCR Detection System and iTaq Universal SYBR Green reagent (Biorad, Hercules, CA, USA). For each gene target, cDNA templates were diluted $10\times$, $100\times$ and $1{,}000\times$ and these dilutions were assayed to verify the linear range of the assay. For routine analyses, 0.2 ng cDNA was used as template. For high copy number transcripts (e.g., 16S rRNA), 0.002 ng of cDNA was used as template. CsCl-cleaned genomic DNA from *M. sedimenti* (diluted over 6 orders of magnitude) provided material for standard curves. Primers and amplification conditions are provided in Supporting Information Table S3. cDNA counts were converted to transcripts per cell as follows: The absolute number of cells harvested in each 20 mL aliquot was inferred from the optical density, assuming that OD_{450} of $0.3 = 5 \times 10^7$ cells (Tavormina *et al.*, 2015). RNA extraction and cDNA conversion were assumed to be constant across samples and assumed to be 100%. The 'starting quantity',

determined by qPCR, was converted to a per ng RNA value, multiplied by the total mass of RNA recovered from the cell pellet, and divided by the total number of cells harvested. 16S rRNA and 'housekeeping' gene transcript levels per cell reported here agreed with estimates from other taxa (e.g., Passalacqua et al., 2009; Milo and Phillips, 2015), in support of this approach.

Headspace gas chromatography-flame ionization detection (GC-FID) analysis

To quantitate methanol accumulation in growth media, duplicate 5 mL samples were removed from duplicate culture vessels and filtered through 0.2 micron syringe filters (EMD Millipore, Fisher Scientific, Pittsburgh PA, USA) into 10 ml Restek headspace crimp vials (Bellafonte, PA, USA). Samples were immediately sealed with aluminium crimps pre-assembled with polytetrafluoroethylene silicone septa. Methanol was analyzed by gas chromatography (GC) on a Restek (Bellafonte, PA, USA) Rtx-VRX 60 m × 0.320 mm ID × 1.8 micron column using flame ionization detection (FID). A Hewlett-Packard 5890 Series II GC with a split-splitless injector (2 mm ID liner) was operated at 200˚C in the splitless mode for 30 s during injection from an HP 7694 Headspace Autosampler. The oven, loop and transfer line of the autosampler were set to 80˚C, 90˚C and 100˚C, respectively, and the GC cycle time was set to 24 min. All other autosampler parameters were left at the factory default values. The post injection split flow was 20 mL/min. Ultra-high purity helium was used for carrier gas, and the column was operated at a constant flow rate of 35 cm/sec average linear velocity. GC oven temperature was held at 35˚C for 6 min, increased 10˚C/min to 60˚C and finally 30˚C/min to 200˚C. The FID was operated at 225˚C.

Electron cryotomography

About 20 mL samples from actively growing and starved cultures were collected by swirling on ice to 4˚C and centrifuging in an Eppendorf 5804R tabletop centrifuge at $2000g$ for 25 min. The supernatant was decanted, and cells were resuspended in 1 mL ice cold PBS (11.8 mM phosphate, 140 mM NaCl) for a final concentration of $\sim 10^8$ cells per mL, and immediately plunge-frozen in liquid ethane-propane cooled to liquid nitrogen temperatures.

Cryotomography of actively growing and methane-starved cells was collected at $22.5\times$ K magnification from −60˚ to 60˚ tilt range, with an angular step of 1˚, a total dose of 200 $e^-/Å^2$, a defocus value of 10 μm, and a final pixel size of 2 nm on a 300-kV FEG G2 Polara transmission electron microscope (TEM) equipped with a lens-coupled 4k-by-4k Ultracam (Gatan, CA) and an energy filter. Data were collected automatically with the UCSF tomography package and reconstructed using the IMOD software package (Kremer *et al.*, 1996). Membrane and S-layer segmentation was performed manually using the Amira software package (Stalling *et al.*, 2005).

References

Arias-Cartin, R., Grimaldi, S., Arnoux, P., Guigliarelli, B., Magalon, A. (2012) Cardiolipin binding in bacterial respiratory complexes: structural and functional implications. *Biochim Biophys Acta* **1817**: 1937–1949.

Benstead, J., King, G.M., and Williams, H.G. (1998) Methanol promotes atmospheric methane oxidation by methanotrophic cultures and soils. *Appl Environ Microbiol* **64**: 1091–1098.

Biller, S.J., Berube, P.M., Lindell, D., Chisholm, S.W. (2015) Prochlorococcus: the structure and function of collective diversity. *Nat Rev Microbiol* **13**: 13–27.

Bodelier, P.L., Gillisen, M.J., Hordijk, K., Damste, J.S., Rijpstra, W.I., Geenevasen, J.A., (2009) A reanalysis of phospholipid fatty acids as ecological biomarkers for methanotrophic bacteria. *ISME J* **3**: 606–617.

Bollmann, A., Schmidt, I., Saunders, A.M., Nicolaisen, M.H. (2005) Influence of starvation on potential ammonia-oxidizing activity and amoA mRNA levels of Nitrosospira briensis. *Appl Environ Microbiol* **71**: 1276–1282.

Case, R.J., Boucher, Y., Dahllof, I., Holmstrom, C., Doolittle, W.F., Kjelleberg, S. (2007) Use of 16S rRNA and rpoB genes as molecular markers for microbial ecology studies. *Appl Environ Microbiol* **73**: 278–288.

Collins, M.D., and Green, P.N. (1985) Isolation and characterization of a novel coenzyme Q from some methane-oxidizing bacteria. *Biochem Biophys Res Commun* **133**: 1125–1131.

DiRusso, C.C., and Nystrom, T. (1998) The fats of Escherichia coli during infancy and old age: regulation by global regulators, alarmones and lipid intermediates. *Mol Microbiol* **27**: 1–8.

Duperron, S., Sibuet, M., MacGregor, B.J., Kuypers, M.M., Fisher, C.R., Dubilier, N. (2007) Diversity, relative abundance and metabolic potential of bacterial endosymbionts in three Bathymodiolus mussel species from cold seeps in the Gulf of Mexico. *Environ Microbiol* **9**: 1423–1438.

Fisher, C.R. (1996) Ecophysiology of primary production at deep-sea vents and seeps. *Biosyst Ecol Ser* **11**: 313–336.

Foster, J.W., and Spector, M.P. (1995) How Salmonella survive against the odds. *Annu Rev Microbiol* **49**: 145–174.

Grupe, B.M., Krach, M.L., Pasulka, A.L., Maloney, J.M., Levin, L.A., Frieder, C.A. (2015) Methane seep ecosystem functions and services from a recently discovered southern California seep. *Mar Ecol* **36**: 91–108.

Hood, M.A., Guckert, J.B., White, D.C., Deck, F. (1986) Effect of nutrient deprivation on lipid, carbohydrate, DNA, RNA, and protein levels in Vibrio cholerae. *Appl Environ Microbiol* **52**: 788–793.

Houser, J.R., Barnhart, C., Boutz, D.R., Carroll, S.M., Dasgupta, A., Michener, J.K., (2015) Controlled measurement and comparative analysis of cellular components in E. coli reveals broad regulatory changes in response to glucose starvation. *PLoS Comput Biol* **11**: e1004400.

Iglesias, A.A., and Preiss, J. (1992) Bacterial glycogen and plant starch synthesis. *Biochem Educ* **20**: 196–203.

Jensen, S., Neufeld, J.D., Birkeland, N.K., Hovland, M., Murrell, J.C. (2008) Methane assimilation and trophic interactions with marine Methylomicrobium in deep-water coral reef sediment off the coast of Norway. *FEMS Microbiol Ecol* **66**: 320–330.

Kato, Y., Fujinaga, K., Nakamura, K., Takaya, Y., Kitamura, K., Ohta, J., et al. (2011) Deep-sea mud in the Pacific Ocean as a potential resource for rare-earth elements. *Nat Geosci* **4**: 535–539.

Kellermann, M.Y., Schubotz, F., Elvert, M., Lipp, J.S., Birgel, D., Prieto-Mollar, X., et al. (2012) Symbiont–host relationships in chemosynthetic mussels: a comprehensive lipid biomarker study. *Organ Geochem* **43**: 112–124.

Keltjens, J.T., Pol, A., Reimann, J., Op den Camp, H. (2014) PQQ-dependent methanol dehydrogenases: rare-earth elements make a difference. *Appl Microbiol Biotechnol* **98**: 6163–6183.

Khmelenina, V., et al. (2010) Structural and functional features of methanotrophs from hypersaline and alkaline lakes. *Microbiologiya* **79**: 498–508.

Khmelenina, V.N., Suzina, N.E., and Trotsenko, Y. A. (2013) Surface layers of methanotrophic bacteria. *Mikrobiologiia* **82**: 515–527.

Kjelleberg, S., Albertson, N., Flardh, K., Holmquist, L., Jouper-Jaan, A., Marouga, R., et al. (1993) How do non-differentiating bacteria adapt to starvation?. *Anton Van Leeuwenhoek* **63**: 333–341.

Kolter, R., Siegele, D.A., and Tormo, A. (1993) The stationary phase of the bacterial life cycle. *Annu Rev Microbiol* **47**: 855–874.

Koynova, R., and Caffrey, M. (1998) Phases and phase transitions of the phosphatidylcholines. *Biochim Biophys Acta* **1376**: 91–145.

Krabbenhoeft, A., Netzeband, G.L., Bialas, J., Papenberg, C. (2010) Episodic methane concentrations at seep sites on the upper slope Opouawe Bank, southern Hikurangi Margin, New Zealand. *Mar Geol* **272**: 71–78.

Kremer, J.R., Mastronarde, D.N., and McIntosh, J.R. (1996) Computer visualization of three-dimensional image data using IMOD. *J Struct Biol* **116**: 71–76.

Ksiazek, K. (2010) Bacterial aging: from mechanistic basis to evolutionary perspective. *Cell Mol Life Sci* **67**: 3131–3137.

Levin, L.A. (2005) Ecology of cold seep sediments: interactions of fauna with flow, chemistry and microbes. In *Oceanography and Marine Biology: An Annual Review.* Gibson, R., Atkinson, R., and Gordon, J. (eds). Boca Raton: Taylor and French. pp. 1–46.

Li, M., Jain, S., Baker, B.J., Taylor, C., Dick, G.J. (2014) Novel hydrocarbon monooxygenase genes in the metatranscriptome of a natural deep-sea hydrocarbon plume. *Environ Microbiol* **16**: 60–71.

Liberton, M., Austin, J.R., 2nd, Berg, R.H., Pakrasi, H.B. (2011) Unique thylakoid membrane architecture of a unicellular N2-fixing cyanobacterium revealed by electron tomography. *Plant Physiol* **155**: 1656–1666.

Linder, K., and Oliver, J.D. (1989) Membrane fatty acid and virulence changes in the viable but nonculturable state of Vibrio vulnificus. *Appl Environ Microbiol* **55**: 2837–2842.

Lindner, A.S., Pacheco, A., Aldrich, H.C., Costello Staniec, A., Uz, I., Hodson, D.J. (2007) Methylocystis hirsuta sp. nov., a novel methanotroph isolated from a groundwater aquifer. *Int J Syst Evol Microbiol* **57**: 1891–1900.

Milo, R., and Phillips, R. (2015) *Cell Biology by the Numbers.* Boca Raton: Taylor & Francis.

Nystrom, T. (2004) Stationary-phase physiology. *Annu Rev Microbiol* **58**: 161–181.

Oliver, J.D., and Stringer, W.F. (1984) Lipid composition of a psychrophilic marine vibrio sp. during starvation-induced morphogenesis. *Appl Environ Microbiol* **47**: 461–466.

Passalacqua, K.D., Varadarajan, A., Ondov, B.D., Okou, D.T., Zwick, M.E., Bergman, N.H. (2009) Structure and complexity of a bacterial transcriptome. *J Bacteriol* **191**: 3203–3211.

Pol, A., Barends, T.R., Dietl, A., Khadem, A.F., Eygensteyn, J., Jetten, M.S., *et al.* (2014) Rare earth metals are essential for methanotrophic life in volcanic mudpots. *Environ Microbiol* **16**: 255–264.

Rao, N.N., Gomez-Garcia, M.R., and Kornberg, A. (2009) Inorganic polyphosphate: essential for growth and survival. *Annu Rev Biochem* **78**: 605–647.

Redmond, M.C., Valentine, D.L., and Sessions, A.L. (2010) Identification of novel methane-, ethane-, and propane-oxidizing bacteria at marine hydrocarbon seeps by stable isotope probing. *Appl Environ Microbiol* **76**: 6412–6422.

Reeburgh, W.S. (2007) Oceanic methane biogeochemistry. *Chem Rev* **107**: 486–513.

Rivers, A.R., Sharma, S., Tringe, S.G., Martin, J., Joye, S.B., Moran, M.A. (2013) Transcriptional response of bathypelagic marine bacterioplankton to the Deepwater Horizon oil spill. *ISME J* **7**: 2315–2329.

Robb, F.T., Sowers, K.R., and Schreier, H.J. (1995) *Archaea: A Laboratory Manual: Methanogens.* Cold Spring Harbor: Cold Spring Harbor Press.

Romantsov, T., Guan, Z., and Wood, J.M. (2009) Cardiolipin and the osmotic stress responses of bacteria. *Biochim Biophys Acta (BBA) - Biomembr* **1788**: 2092–2100.

Ruff, S.E., Arnds, J., Knittel, K., Amann, R., Wegener, G., Ramette, A., *et al.* (2013) Microbial communities of deep-sea methane seeps at Hikurangi continental margin (New Zealand). *PLoS One* **8**: e72627.

Siegele, D.A., and Kolter, R. (1992) Life after log. *J Bacteriol* **174**: 345–348.

Stalling, D., Westerhoff, M., and Hege, H.C. (2005) Amira: a highly interactive system for visual data analysis. In *The Visualization Handbook.* Hansen, C., and Johnson, C. (eds). New York: Elsevier. pp. 749–767.

Sturt, H.F., Summons, R.E., Smith, K., Elvert, M., Hinrichs, K.U. (2004) Intact polar membrane lipids in prokaryotes and sediments deciphered by high-performance liquid chromatography/electrospray ionization multistage mass spectrometry–new biomarkers for biogeochemistry and microbial ecology. *Rapid Commun Mass Spectrom* **18**: 617–628.

Tavormina, P.L., Hatzenpichler, R., McGlynn, S., Chadwick, G., Dawson, K.S., Connon, S.A., *et al.* (2015) Methyloprofundus sedimenti gen. nov., sp. nov., an obligate methanotroph from ocean sediment belonging to the 'deep sea-1' clade of marine methanotrophs. *Int J Syst Evol Microbiol* **65**: 251–259.

Tocheva, E.I., Li, Z., and Jensen, G.J. (2010) Electron cryotomography. *Cold Spring Harb Perspect Biol* **2**: a003442.

Tocheva, E.I, Dekas, A.E, McGlynn, S.E, Morris, D, Orphan, V.J, Jensen, G.J. (2013) Polyphosphate storage during sporulation in the gram-negative bacterium Acetonema longum. *J Bacteriol* **195**: 3940–3946.

von Deimling, J.S., Greinert, J., Chapman, N.R., Rabbel, W., Linke, P. (2010) Acoustic imaging of natural gas seepage in the North Sea: Sensing bubbles controlled by variable currents. *Limnol Oceanogr: Methods* **8**: 155–171.

Wang, L., and Wise, M.J. (2011) Glycogen with short average chain length enhances bacterial durability. *Naturwissenschaften* **98**: 719–729.

Wörmer, L., Lipp, J.S., Schröder, J.M., Hinrichs K-U. (2013) Application of two new LC–ESI–MS methods for improved detection of intact polar lipids (IPLs) in environmental samples. *Organ Geochem* **59**: 10–21.

Wu, M.L., van Teeseling, M.C., Willems, M.J., van Donselaar, E.G., Klingl, A., Rachel, R., *et al.* (2012) Ultrastructure of the denitrifying methanotroph "Candidatus Methylomirabilis oxyfera," a novel polygon-shaped bacterium. *J Bacteriol* **194**: 284–291.

Yoshinaga, M.Y., Kellermann, M.Y., Rossel, P.E., Schubotz, F., Lipp, J.S., Hinrichs, K.U. (2011) Systematic fragmentation patterns of archaeal intact polar lipids by high-performance liquid chromatography/electrospray ionization ion-trap mass spectrometry. *Rapid Commun Mass Spectrom* **25**: 3563–3574.

Supporting information

Additional supporting information may be found in the online version of this article at the publisher's web-site.